Shear capacity of ASR damaged structures – in-depth analysis of some in-situ shear tests on bridge slabs

Hansen, Søren Gustenhoff; Barbosa, Ricardo Antonio; Hoang, Linh Cao; Hansen, Kurt Kielsgaard

Published in:
Proceedings of the 15th international conference on alkali-aggregate reaction in concrete (15th ICAAR)

Publication date:
2016

Document Version
Peer reviewed version

SHEAR CAPACITY OF ASR DAMAGED STRUCTURES – IN-DEPTH ANALYSIS OF SOME IN-SITU SHEAR TESTS ON BRIDGE SLABS

Søren G. Hansen[1]*, Ricardo A. Barbosa[2], Linh C. Hoang[2], Kurt K. Hansen[2]

[1]Dept. Of Technology and Innovation, Faculty of Engineering, University of Southern Denmark, DENMARK

[2]Dept. of Civil Engineering, Technical University of Denmark, DENMARK

Abstract

This paper deals with the influence of alkali-silica reaction (ASR) on the shear capacity for concrete slabs without shear reinforcement. An experimental full-scale in-situ program consisting of four slabs from a bridge (Vosnæsvej) has been carried out and the results have been published in ref. [1] with the principal author of this paper as co-author. After the experiments, a detailed measurement of the test specimens was conducted. Based on these measurements a thorough analysis of the experimental results was carried out and evaluated by a plastic model for shear capacity, Crack Sliding Model (CSM) and Eurocode 2 (EN 1992-1-1). The analysis shows that three experiments were highly affected by the preparation of the experimental setup. Only one experiment contained useful information about the shear capacity. The analysis of this experiment shows that the shear capacity is not reduced as much as the measured concrete compressive strength indicates. Furthermore, the analysis shows that the ASR-induced prestress may be the reason for this phenomenon.

Keywords: Alkali Silica Reaction, Shear Capacity, Full Scale testing, Crack Sliding Model, Failure Analysis

1 INTRODUCTION

In Denmark, several bridges are severely damaged due to alkali silica reaction (ASR) and more than 600 bridges have the potential to develop ASR deterioration due to lack of maintenance and reactive aggregates used in the concrete, [1]. ASR damages in bridges and dams have been observed worldwide [2]. Unfortunately, there is no commonly accepted method to assess the residual load carrying capacity of these ASR-damaged structures. The theories and models for capacity calculations prescribed in standards and codes are mainly developed as (conservative) design tools for new structures and not intended for assessment of damaged structures. As a consequence, the engineers are in many situations left with rough estimates on the residual load carrying capacity without empirical evidence. The lack of knowledge may have caused unnecessary expensive replacements, repairs or even worse unsatisfactory structural safety.

In 2012, the Danish Road Directorate initiated an in-situ full-scale test program to assess the shear capacity of a non-shear reinforced concrete bridge deck (the Vosnæsvej Bridge) suffering from ASR deteriorations. Results of the full-scale tests and laboratory compressive tests on vertical drilled cores were published in 2014 [1] where the tested capacity was compared with the shear strength equation in Eurocode 2. Since then, additional as well as more thorough investigations of the "as built" reinforcement layout and material properties have been conducted. This paper offers a re-examination of the tested load carrying capacities based on the newly gained information on material properties and "as built" reinforcement layout. Furthermore, calculations of the shear capacity by mean of a plasticity based model are presented.

* Correspondence to: SGH@iti.sdu.dk

2 MATERIALS AND METHODS

2.1 The Bridge

The Vosnæsvej Bridge was constructed in 1976 as an in-situ cast structure consisting of two 3-span continuous prestressed main beams supporting an integrated deck without shear reinforcement. The bridge is approximately 10 m wide and 55 m long with a maximum span of approximately 27 m. According to the design drawings, the concrete cover is 30 mm.

In 2012 visual inspections showed severe ASR crack formation in the cantilevered part of the deck and in the prestressed main beams. The shear capacity of the bridge deck was the main concern due to the absence of shear reinforcement.

According to the design drawings the original characteristic concrete compressive strength is 30 MPa. This corresponds to an estimated mean compressive strength on the day of experiments of 45.6 MPa using [3], [4] and [5].The reinforcement is specified as deformed bars with a characteristic yield stress (0.2% stress) of 560 MPa.

In Denmark the most bridges suffering from ASR-deteriorations are built with fast reactive aggregates in the sand fraction.

2.2 Experimental Setup – Shear tests

Four in-situ full-scale shear tests were performed on the northern cantilevered part of the bridge, named VV1, VV2, VV3 and VV4. The residual shear capacity was tested on 1 m wide strips of the cantilevered slab, which were cut free on three sides. The test specimens (strips) were only restrained in the main beams. The size of the test specimens and the experimental setup are shown in Figure 1. Additionally, the figure shows that the load was applied 900 mm from the restrained end by a spreader beam (HE300B profile) to ensure a one-way shear action in the specimens. The load was applied by a hydraulic actuator, oil flow controlled, (i.e. not fully load nor fully deformation controlled). Further details about the experimental setup are described in [1].

2.3 Concrete – Strength and ASR-induced cracks

After the shear tests were conducted and published, [1], additional tests and analysis were conducted to assess the concrete condition and ASR deterioration. To assess the ASR deterioration, an impregnation with fluorescent epoxy was performed on a surface of a test specimen (the cut counterpart surface) [6]. Figure 2 shows this impregnation, where it can be seen that there is well-defined horizontal cracks. The concrete strength was measured on cores drilled directly from the bridge deck and from beams cut during the preparation of the shear tests. The cores drilled directly from the deck had a diameter of 150 mm and a height of 150 to 300 mm. The cores drilled from the beams had a diameter of 100 mm and a height of 150 to 200 mm. To study the influence of crack direction (identified on the epoxy impregnation) on the compressive strength cores were drilled horizontally and vertically. The vertically drilled cores had cracks perpendicular to the load direction and the horizontally drilled cores had cracks parallel to the load direction. All tests of compressive strength were conducted as deformation controlled with a rate of 0.5 mm/min. The test results were converted to strength for a standard cylinder (150 x 300 mm) using a guideline from The Danish Road Directorate, as described in [6]. In this paper the compressive strength are based on all size of concrete cores.

All laboratory analyses were conducted at the Technical University of Denmark, Department of Civil Engineering.

2.4 Reinforcement – Mapping and Strength

To understand the results of the shear tests a detailed mapping of the "as built" top side reinforcement was performed. Figure 3 shows the mapped reinforcement. The reinforcement was almost as shown on the design drawings (T20/250 mm). However, the mapping reveals that several reinforcement bars were accidentally cut during the preparation of the shear tests where the spreader beam had to be installed.

23 undamaged reinforcement bars of 600 mm were cut free of the four test specimens and used to measure the tensile strength. The strain of the reinforcement bars was measured over 50 mm and the load was applied as oil flow controlled. The measurements did not show a clear yield plateau on the stress-strain curves. Thus, the yield stress is defined as the 0.2% stress.

2.5 Methods for calculation of shear capacity

Crack Sliding Model

To analyse the shear capacity of the specimens we have used the Crack Sliding Model (CSM). CSM is based on the upper bound theorem of plasticity and was originally developed for prediction of shear capacity of beams without shear reinforcement, [7].

Based on a rigid body failure mechanism where all plastic deformation is assumed to take place in an inclined crack, the model provides an expression for the sliding resistance in this crack characterised by its horizontal projection x, see Figure 4.

$$V_u(x) = \tfrac{1}{2}\nu f_c b h\left(\sqrt{x^2+h^2} - x\right) \qquad \text{for } \frac{\Phi}{\nu} \geq \frac{1}{2} \tag{1}$$

In Eq. (1), b and h are respectively the width and height of the cross section, f_c is the concrete compressive strength, $\Phi = A_s f_y / b h f_c$ is the mechanical reinforcement ratio and ν is a so-called effectiveness factor for cracked concrete:

$$\nu = \frac{0.44}{\sqrt{f_c}}\left(1 + \frac{1}{\sqrt{h}}\right)(1 + 26\rho); \qquad h \text{ in meters and } f_c \text{ in MPa} \tag{2}$$

where $\rho = A_s / bh$ is the reinforcement ratio.

The expression assumes that the shear failure occurs along an existing crack. Therefore, an additional failure criterion is considered; namely the cracking criterion. Based on a rotational cracking mechanism the model provides an expression for the cracking criterion:

$$V_{cr}(x) = \frac{\frac{1}{2} f_{tef} b (x^2+h^2)}{a} + N\frac{e}{a} \tag{3}$$

where a is shear span (see Figure 4), e is the distance from the top face to the normal force and f_{tef} is the effective concrete tensile strength:

$$f_{tef} = 0.156 f_c^{\frac{2}{3}} \left(\frac{h}{0.1}\right)^{-0.3}, \; h \text{ in meters} \tag{4}$$

Figure 5 shows a graphical presentation of the two criterions; i.e. the sliding criterion and the cracking criterion. Since the sliding criterion is based on an upper bound approach the lowest possible strength is the capacity. However, the expression for the sliding criterion is only valid if the cracking criterion is fulfilled as well. This means that the shear capacity is found as the intersection between the two criteria, which in addition gives an estimate of the horizontal projection of the critical crack (in the following called x_{cri}). From Figure 5 it can be seen that a normal force will increase the cracking criterion which entails that the shear capacity will increase and x_{cri} will decrease. For a comprehensive and more detailed explanation of CSM, see [7] and [8].

The shear strength equation in EN1992-1-1 for members without shear reinforcement

The calculations in this paper according to Eurocode 2 are based on the rules in EN1992-1-1 [4] and the associated Danish Annex [5]. According to Eurocode 2 we need to consider all sections in the slab. Because the shear force is constant for this experimental setup the smallest structural height should be used. However, we know from CSM that the largest structural height will be activated, which is confirmed by the observed failure mechanisms in the experiments. Thus the largest structural height is used in the calculations in this paper. The Eurocode 2 shear strength equation is empirical and requires that the tensile reinforcement is fully anchored. The calculations in this paper assume that this requirement is fulfilled.

The shear strength equation of Eurocode 2 is included in this paper primarily to assess the tested results in a manner that most engineers in practice without ASR knowledge will do.

3 RESULTS

The calculations presented in this paper are based on the mean of all measured concrete compressive strengths and the mean yield strength of the reinforcement. Additionally, the self-weight of the specimens is neglected.

Compressive strength of concrete cores

TABLE 1 shows the compressive concrete strength of horizontally and vertically drilled cores. It can be seen that the measured mean strengths are significantly lower than the estimated mean compressive strength for undamaged concrete (45.6 MPa). In [6] the influence of the crack orientation on the concrete properties is discussed.

Reinforcement

The tensile tests of the steel reinforcement showed a mean yield stress (0.2% stress) of 646.4 MPa with a sample standard deviation of 45.9 MPa. The mean ultimate stress is 716.1 MPa with a sample standard deviation of 19.5 MPa.

In-situ shear tests

TABLE 2 shows the measured failure loads from the in-situ full-scale shear tests [11]. Besides of the failure load (V_u), TABLE 2 shows the ratio between the failure load and the predicted shear capacity based on CSM ($V_{R,CSM}$) and Eurocode ($V_{R,EC2}$). Furthermore, the table shows the ratio between the bending moment corresponding to the failure load (M_U) and the predicted bending capacity (M_R). Finally, the figure specifies the reinforcement and the slab width used in the calculations. From the table it is seen that specimen VV2 has a significantly lower failure load than the rest of the test specimens. Specimen VV2 is the only slab, which had a lower failure load than predicted by the CSM. It seems that Eurocode is more conservative than CSM.

Figure 6 to 9 show the crack pattern on the two sides of the four tested specimens. In the figures the load-induced crack which governed the failure load, i.e. the critical crack, is marked. Furthermore, the horizontal projection of the large cracks is specified. The following can be observed:

- Specimen *VV1*: The horizontal projection of the critical crack is approximately symmetric (790 mm vs. 810 mm). However, the crack pattern is a bit different the two surfaces between. The critical crack propagates from the fixed support to the load plate.
- Specimen *VV2*: The crack orientation and crack pattern are approximately symmetric while the crack width is strongly larger on the eastern surface than on the western surface. The critical crack propagates from the fixed support to the load plate.
- Specimen *VV3*: The crack pattern is symmetric. The critical crack propagates from the fixed support with a horizontal projection of 520 mm.
- Specimen *VV4*: The crack pattern is almost symmetric while the crack width is slightly larger on the western surface than on the eastern surface. The critical crack propagates from the fixed support with a horizontal projection of 520-570 mm. In addition, bending cracks are visible on both surfaces.

Figure 10 shows the load-displacement curves for all four test specimens as reported in [1]. For specimen VV1 it can be seen that the capacity decreases after reaching the peak load. For specimen VV2 a significantly lower peak load is observed but there is no drop in the response after the peak load and a ductile failure is obtained. Specimen VV3 behaved brittle with a sudden post peak drop. Specimen VV4 had a ductile failure where the load stays constant after reaching the peak load. However, after a while, a sudden drop of load from approximately 450 kN to 330 kN took place.

4 DISCUSSION

4.1 Specimen VV1

The results from the experiment for VV1 show:

- The failure load is a bit larger than predicted by CSM, TABLE 2.
- The moment corresponding to the failure load is a bit larger than the calculated moment capacity, TABLE 2.
- No bending cracks were observed, Figure 6.
- The critical crack propagates to the load plate, Figure 6.
- Two T20 reinforcement bars were cut during the preparation of the experimental setup, Figure 3.
- A quasi-brittle behaviour at failure, Figure 10.

The fact that no bending cracks occurred during the experiment strongly indicates a presence of an ASR-induced prestressing effect in the reinforcement. Because of the cut rebars the prestressing and the moment capacity are reduced near the load plate. Therefore, the failure might be initiated by bending failure and a wide inclined crack will occur. It is well-known that the shear capacity of a crack decreases as function of the crack width (see e.g. [9]); thus a non-ductile shear failure may have taken place after formation of the crack and yielding of the bars. Despite the failure mechanism looks like a shear failure, is the failure load not an expression of a shear capacity.

4.2 Specimen VV2

The results from the experiment for VV2 show:

- The failure load is significantly lower than predicted by the CSM and the bending capacity, TABLE 2.
- No bending cracks were observed, Figure 6.
- The crack width on the two surfaces was significantly different, Figure 6.
- The critical crack propagates to the load plate, Figure 6.
- Two T20 reinforcement bars were cut during the preparation of the experimental setup, Figure 3.
- A ductile behaviour at failure, Figure 10.

As for specimen VV1, the absence of bending cracks strongly indicates a presence of an ASR-induced prestressing effect in the reinforcement. Also in specimen VV2, the prestressing and the moment capacity are reduced near the load plate due to cut reinforcement. However, since specimen VV2 only has two uncut T20 rebars (in the western side) left, the moment capacity is drastic reduced for an inclined crack. A thorough inspection of the critical crack showed that all four reinforcement bars went through the crack but two had a very short anchorage. In fact, the failure load (285.8 kN) is in close agreement with a bending capacity which is calculated by including only three reinforcement bars (271.6 kN). Therefore, the failure is probably a bending failure in an asymmetric reinforced section. This explains the coarse crack on the western surface and the ductile behaviour shown in Figure 10. Despite the crack looks like a shear crack, is the failure load not an expression of a shear capacity.

4.3 Specimen VV3

The results from the experiment for VV3 show:

- The failure load corresponds very fine with the predicted CSM shear capacity and bending capacity, TABLE 2.
- No bending cracks were observed, Figure 6.
- The crack width on the two surfaces was significantly different, Figure 6.
- The critical crack propagates from the fixed support with a horizontal projection of 520 mm, Figure 6.
- All reinforcement bars were cut during the preparation of the experimental setup, Figure 3.
- A brittle behaviour at failure, Figure 10.

As for specimens described above, the absence of bending cracks strongly indicates a presence of an ASR-induced prestressing effect in the reinforcement. For specimen VV3, the prestressing and the moment capacity (cracked section) are also reduced near the load plate due to cut reinforcement.

To form the inclined crack with a reduced moment capacity, the moment capacity for uncracked concrete must be exceeded. In this case, the moment capacity for the uncracked concrete might be higher than the moment capacity for cracked concrete. Since the moment capacity of uncracked concrete is controlled by the concrete tensile strength, a brittle behaviour at failure is expected. However, the failure can also shear failure. Due to the cut rebars, we cannot determine whether this failure load is an expression for the shear capacity or the uncracked moment capacity (cracking criterion in CSM). However and despite of fine agreement with CSM, the experiment does not contain information of how the ASR-induced prestressing effect affects the residual shear capacity.

4.4 Specimen VV4

The results from the experiment for VV4 show:

- The failure load is significantly larger than the expected failure load predicted by CSM and bending capacity. TABLE 2.
- Bending cracks were observed, Figure 6.
- The crack width on the two surfaces was significantly different, Figure 6.
- The critical crack propagates from the fixed support with a horizontal projection of 520-570 mm.
- No reinforcement bars were cut during the preparation of the experimental setup, Figure 3.
- A ductile behaviour at failure, Figure 10.

The failure is a combined shear and bending failure. The bending failure explains the ductile behaviour and the shear failure explains the inclined crack.
According to CSM, the sliding resistance of a crack with a horizontal projection of 545 mm (the average x_{cri}) is 497.6 kN. This result agrees with the failure load of 496.1 kN. CSM underestimate the cracking criterion for this crack. This shows that the ASR-induced prestressing effect has a crucial effect on the residual shear capacity. The presence of bending cracks can be explained by the higher failure load.

4.5 General

The shear capacity for specimen VV4 is significantly larger than the shear capacity predicted on the basis of the measured reduced concrete compressive strength (approximately 30% larger than result of CSM and 93% larger than result according to Eurocode). It seems too conservative to use CSM or Eurocode with reduced concrete compressive strength without the ASR-induced prestressing. Despite that specimen VV1, VV2 and VV3 do not contain important information about the shear capacity; they also indicate a presence of an ASR-induced prestressing effect in the reinforcement.

The effect of ASR-induced prestress has indeed before in the literature [10] been used to explain surprisingly high tested shear capacity for ASR deteriorated beams. However, the results in [10] are based on laboratory prepared and exposed concrete beams, and not real-life ASR damaged structure. To the best knowledge of the authors, this paper is the first study that shows a strong indication of the major influence of a prestressing effect on the shear capacity of real life ASR damaged structures based on an analysis of tested material properties.

By means of the Crack Sliding Model, residual strength was predicted satisfactory when the calculation is based on an observed critical crack. Yet, in order to develop a shear model that takes ASR-effects into account we need more test results from slab elements and more knowledge about the ASR-induced prestressing effect.

If it is the ASR-induced prestressing effect that in fact ensures sufficient residual shear capacity in general, a special attention must be payed to prestressed structures. Since the prestressing effect on shear capacity is limited up until a certain level. In that case, additional ASR-induced prestress of the reinforcement may not ensure the residual shear capacity to the same extent as for conventionally reinforced concrete structures suffering ASR.

5 CONCLUSION

This paper provided a more indebt analysis of the results of some in-situ shear tests on an ASR-damaged bridge, [1]. It has been argued, that only one experiment may be considered as a true shear test. The remaining tests were affected by the circumstance that the main reinforcement bars were unintentionally cut during the test preparation. This resulted in tests, where the specimens suffered a kind of bending/anchorage failure. However, all experiments indicate a presence of an ASR-induced prestressing effect in the reinforcement.

The one test available for further analysis showed a residual shear capacity, that is about 30% higher as the capacity of an undamaged beam having the same compressive concrete strength as the measured strength for this particular bridge. By means of the Crack Sliding Model, this residual strength was predicted satisfactory when the calculation is based on a observed critical crack.

6 ACKNOWLEDGEMENT

The authors thank Ninnie Eiken Abildgaard and Jakob Fogdal for their great work and interest during their master's thesis work concerning shear capacity for concrete structures suffering from ASR deterioration.

7 REFERENCES

[1] Schmidt JW, Hansen SG, Barbosa RA, Henriksen A (2014): Novel shear capacity testing of ASR damaged full scale concrete bridge, Engineering Structures, 79

[2] Wigum BJ, Pedersen LT, Grelk B, Lindgård J (2006): State-of-the art report: key parameters influencing the alkali aggregate reaction, SINTEF Building and Infrastructure

[3] The Danish Road Directorate (2010): Vejledning til belastning- og beregningsgrundlag (in Danish)

[4] European Standard (2008): Eurocode 2. Design of concrete structures - Part 1-1-: General rules and rules for buildings

[5] Dansk Standard (2013): The Danish National Annex for Eurocode 2

[6] Barbosa, RA and Hansen KK (2014): The influence of Alkali-Silica Reaction and Crack Orientation on the Mechanical Properties of Concrete. Proc. of the 10th fib International PhD Symposium in Civil Engineering, Quebec, Canada

[7] Zhang JP (1994): Strength of Cracked Concrete, Part 1 - Shear Strength of Conventional Reinforced Concrete Beams, Deep Beams, Corbels and Prestressed Reinforced Concrete Beams without Shear Reinforcement, PhD thesis, Department of Structural Engineering and Materials, Technical University of Denmark, Series R, No 311.

[8] Nielsen MP, Hoang LC (2011): Limit Analysis and Concrete Plasticity, 3rd edition, CRC Press

[9] Muttoni A, Ruiz MF (2008): Shear Strength of Members without Transverse Reinforcement as Function of Critical Shear Crack Width, ACI Structural Journal, 105.2

[10] The Road Directorate, The Bridge Department (1990): Load carrying capacity of members subjected to alcali silica reactions, Ministry of Transportation

[11] Fogdal J, Eiken N (2013): Shear Capacity of Concrete Structures Subjected to Alkalisilica Reactions (In Danish), Master Thesis, University of Southern Denmark, Faculty of Engineering.

TABLE 1: Compressive concrete strength, f_c, for the four specimens in vertical and horizontal drilling direction. The strength is specified as a mean (μ), a standard sample deviation (σ) and the number of cylinders in the sample.

Test	Vertical			Horizontal			Overall		
	μ [MPa]	σ [MPa]	Samples	μ [MPa]	σ [MPa]	Samples	μ [MPa]	σ [MPa]	Samples
VV1	21.7	7.7	8	25.2	2.3	3	22.6	6.7	11
VV2	28.2	6.7	5	24.1	1.3	3	26.6	5.5	8
VV3	26.7	5.8	9	27.1	7.7	3	26.8	5.9	12
VV4	28.1	8.7	14	30.6	3.4	5	28.8	7.6	19
Total	26.4	7.7	36	27.3	4.6	14	26.6	7.0	50

TABLE 2: Failure load, tension reinforcement, section width and shear and moment utility. Failure load, reinforcement and section width are adapted from [11].

Test	Failure load [kN] V_u	Tension Reinforcement	Section width [mm]	$V_u/V_{R,CSM}$	$V_u/V_{R,EC2}$	M_u/M_R
VV1	440.8	4T20 + 1T16	1020	1.14	1.63	1.07
VV2	285.8	4T20	1040	0.73	1.10	0.80
VV3	402.3	4T20	1020	1.05	1.56	1.12
VV4	496.1	4T20	1020	1.29	1.93	1.39

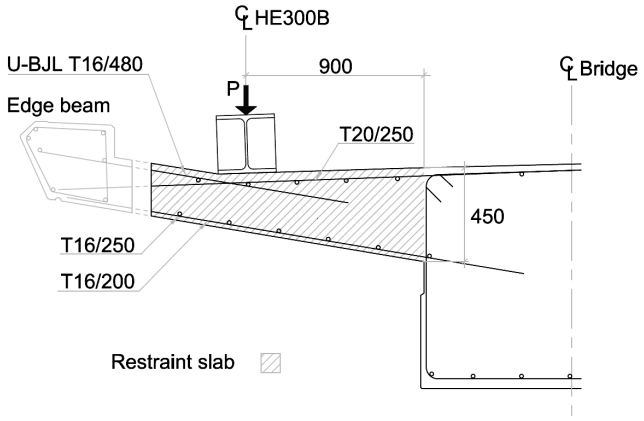

FIGURE 1: Size of test specimen ad experimental setup, adapted from [11].

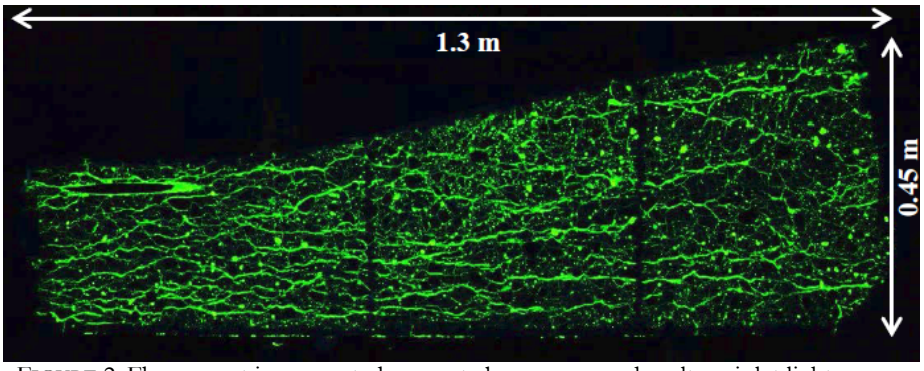

FIGURE 2: Fluorescent impregnated concrete beam seen under ultra-violet light. Experiment VV4. From [6].

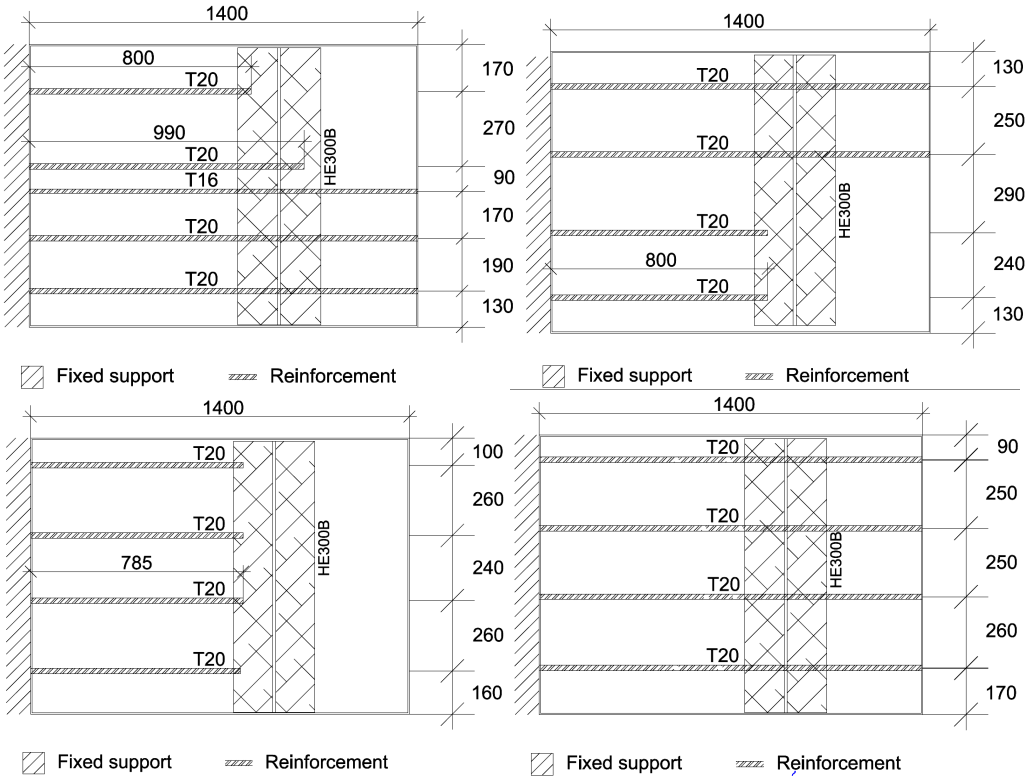

FIGURE 3: Detailed measurement of the upside reinforcement (tension), Upper left: VV1; Upper right: VV2; Lower left: VV3; Lower left: VV4; all dimensions are specified in mm. Adapted from [11].

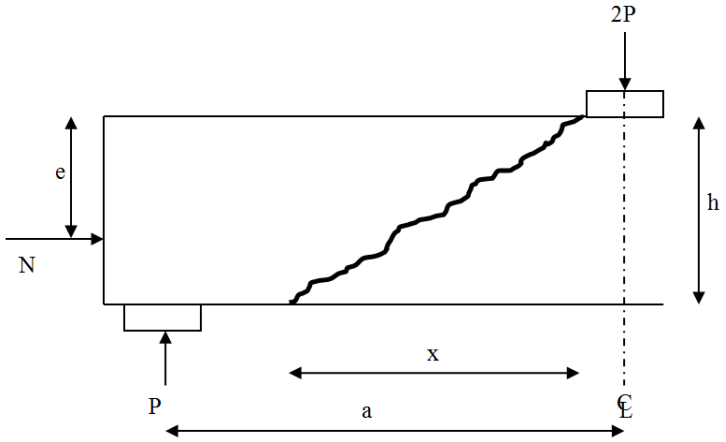

FIGURE 4: Shear failure mechanism in beam with a normal force.

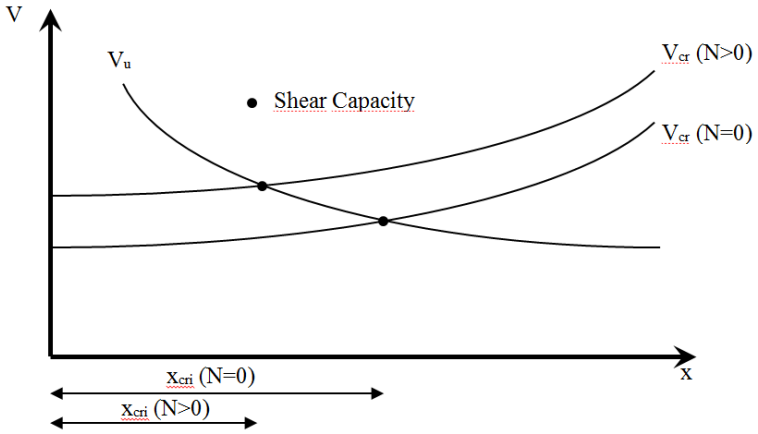

FIGURE 5: Graphical presentation of the sliding criterion, V_u, and the cracking criterion, V_{cr}.

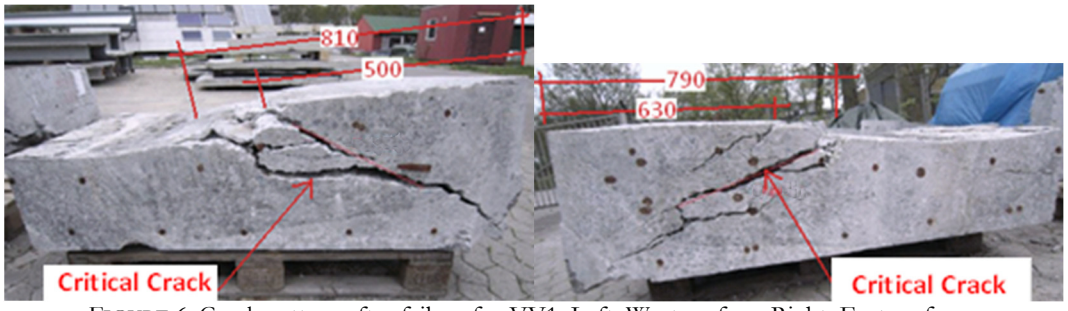

FIGURE 6: Crack pattern after failure for VV1. Left: West surface. Right: East surface. All measures are given in mm. Adapted from [11].

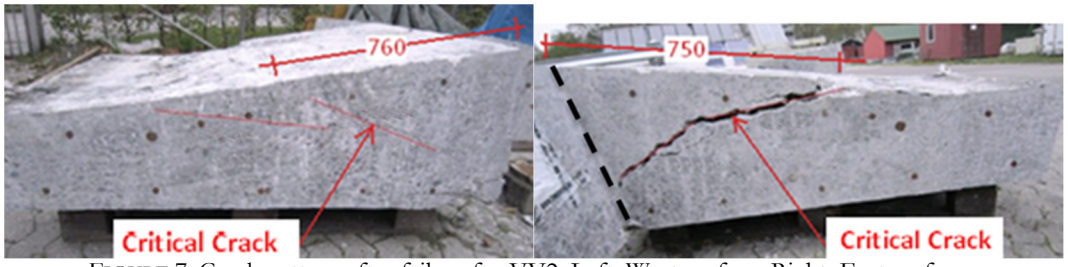

FIGURE 7: Crack pattern after failure for VV2. Left: West surface. Right: East surface. All measures are given in mm. NOTE: Not the full eastern surface is visible, limited by the dashed line. Adapted from [11].

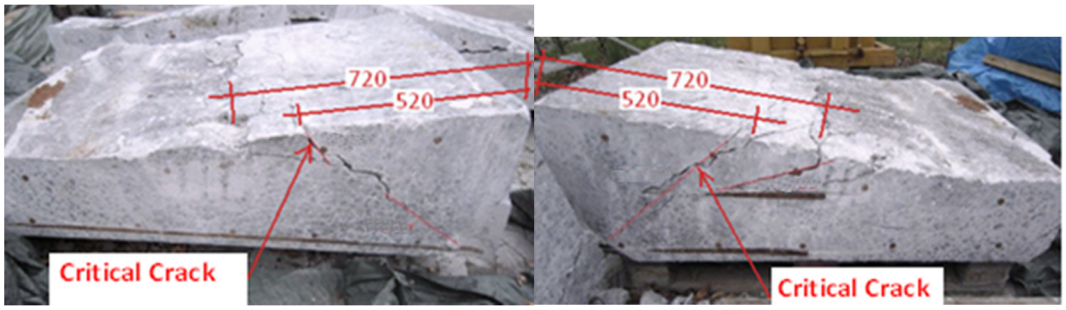

FIGURE 8: Crack pattern after failure for VV3. Left: West surface. Right: East surface. All measures are given in mm. Adapted from [11].

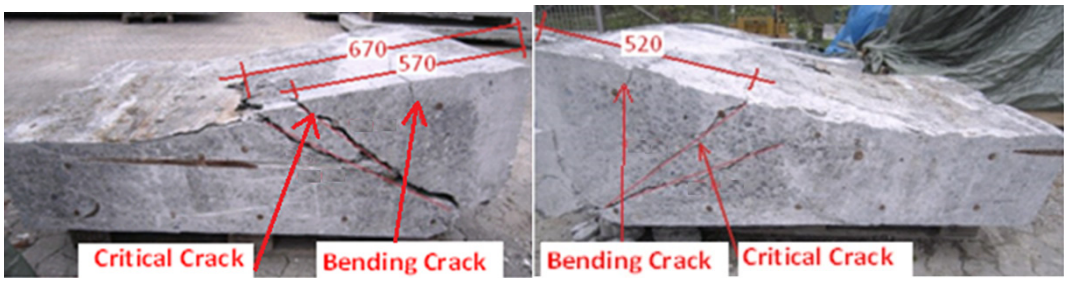

FIGURE 9: Crack pattern after failure for VV4. Left: West surface. Right: East surface. All measures are given in mm. Adapted from [11].

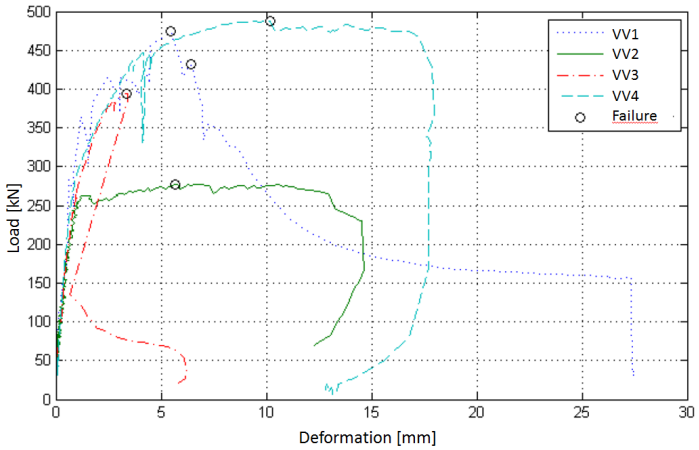

FIGURE 10: Load-displacement curves for each specimen. Adapted from [11].